

Supporting Information

Transformation of PAHs and Formation of Environmentally Persistent Free Radicals on Modified Montmorillonite: Role of Surface Metal Ions and PAH Molecular Properties

Hanzhong Jia^{a,b}, Song Zhao^b, Yafang Shi^a, Lingyan Zhu^a, Chuanyi Wang^b, and
Virender K. Sharma^{c*}

^a Key Laboratory of Plant Nutrition and the Agri-environment in Northwest China,
Ministry of Agriculture, College of Natural Resources and Environment,
Northwest A & F University, Yangling 712100, China.

^b Xinjiang Technical Institute of Physics & Chemistry, Chinese Academy of Sciences,
Urumqi 830011, China.

^c Program for the Environment and Sustainability, Department of Occupational and
Environmental Health, School of Public Health, Texas A&M University,
College Station, TX 77843, USA.

Total Pages: 15

Text: 5

Table: 3

Figures: 7

Text S1. Anhydrous ferric chloride (FeCl_3), copper chloride (CuCl_2), nickel chloride (NiCl_2), cobalt chloride (CoCl_2), zinc chloride (ZnCl_2), sodium chloride (NaCl), sodium acetate (NaAc), sodium hydroxide (NaOH), sodium diphosphate ($\text{Na}_4\text{P}_2\text{O}_7$), hydrochloride acid (HCl , 36~38 %), and chemically pure sodium chloride (NaCl) were obtained from Sinopharm Chemical Reagent Co., Ltd (Shanghai, China). Phenanthrene (PHE, 98%), anthracene (ANT, 98%), benzo[a]anthracene (B[a]A, 98%), pyrene (PYR, 98%), and benzo[a]pyrene (B[a]P, 96%) and methanol (HPLC-grade solvent) were purchased from J&K Chemical (Beijing, China). All the chemicals were used as received without further purification.

Text S2. Metal contents in original montmorillonite clays and metal ions loading clays were quantified using an inductively coupled plasma-atomic emission spectroscopy (ICP-AES) technique. An instrument used was Thermo-ICAP6300 (Waltham, USA). In this experimental set-up, samples were prepared by thermal-digestion at 250 °C in the mixture of nitric acid (5 ml, 65%), hydrofluoric acid (5 ml, ~ 38%), and hydrochloric acid (10 ml, 37%) for 90 min. The differences of individual metal content between original clay and modified clays were 0.56, 0.76, 0.74, 0.75, and 0.69 mmol g^{-1} for Fe(III), Cu(II), Ni(II), Co(II), and Zn(II), respectively.

To investigate the change of the basing spacing during the preparation of clay samples, samples of original clay, modified clays, and PAHs-contaminated clays were investigated by a X-ray diffraction (XRD) technique. The XRD instrument used in this study was Bruker D8-Advance (Karlsruhe, Germany), equipped with $\text{CuK}\alpha$ radiation ($\lambda = 1.54178 \text{ \AA}$) and a crystal graphite monochromator, operating at 40 kV and 40 mA. The XRD signals were collected with diffraction angles ranging from 4

and 20 ° at a scanning rate of 1° min⁻¹. The basal spacing of clay minerals was calculated using the Bragg equation (Eq. 1)

$$d(001) = 1.54178 / (2 \sin (\theta/2)) \quad (1)$$

where d(001) refers to the basal spacing of smectite clays, and θ is the incident angle.

Text S3. The possible change in relative humidity (RH) during the sample taken from petti dish and quenching the reaction (i.e., less than 1 minute time period) was systematically tested. In this experimental set-up, we compared the reaction systems with or without sampling at preselected time. In this study, “without sampling” stands for not opening the desiccator until the end point. As shown in Figure S3, no significant difference was determined for the transformation of target PAH and subsequent formation of EPFRs. Hence, the change of RH during the sampling (opening the desiccator) had no influence on obtained results in our study.

Text S4. The concentrations of PAHs in the extract were quantified using a Thermo Fisher Ultra 3000 HPLC equipped with a 25 cm × 4.6 mm Cosmosil C18 column (Waltham, Massachusetts, United States). A 85:15 (v/v) mixture of methanol:water was employed as the mobile phase solvent. The flow rate was 1.0 mL min⁻¹, and the ultraviolet detector (Thermo Fisher, Waltham, Massachusetts, United States) was set at 254 nm.

The transformation intermediate products were identified using an Agilent 7890A-5975C gas chromatograph-mass spectrometer (Santa Clara, California, United States). The mass spectrometer was operated on a full scan mode (30–500 amu), and was equipped with a HP-5MS capillary column (length = 30 m; internal diameter = 250 μ m; film thickness = 0.25 μ m) (Santa Clara, California, United States). Helium

was the carrier gas at a flow rate of 1.2 mL min⁻¹ with splitless injection at 230 °C. To detect the products of PAHs, the oven temperature was programmed from 80 °C to 200 °C (20 °C min⁻¹, 2 min hold), then to 260 °C (20 °C min⁻¹, 2 min hold), and then to 310 °C (20 °C min⁻¹, 2 min hold).

Text S5. Measurements of electron paramagnetic resonance (EPR) spectra were performed using a Bruker E500 EPR spectrometer (Karlsruhe, Germany). All of samples were analyzed at room temperature with an X-band microwave frequency of 9.7 GHz, microwave power of 2.02 mW, and modulation amplitude of 4.00 G. Instrument and operating parameters were set as follows: at center field, 3470 G; modulation amplitude, 4.0 G; sweep width, 200 G; receiver gain, 3.54*10⁴; time constant, 41.0 ms; and sweep time, 167.7 s. Radical concentrations were calculated by comparing the signal peak area, as derived from $(\Delta H_{p-p})^2$ multiplied by the relative intensity, to a 2,2-diphenyl-1-picrylhydrazyl standard.

To monitor the spectral changes of the PAH molecules, a Perkin-Elmer Lambda 4C diffuse reflectance UV-visible spectroscopy with a scattered transmission accessory (Waltham, Massachusetts, United States) was also used to measure the interaction of PAHs with metal ion-modified clays.

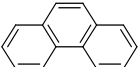
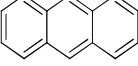
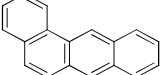
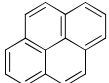
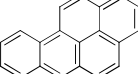
X-ray photoelectron spectroscopy analysis was by an ESCA-Lab-250i-Xi XPS spectrometer (Shimadzu Co., Japan). This instrument consisted monochromatic Al K α radiation (180 W, 12 mA, 15 kV) and diameter beam spot of 500 mm.

Table S1. The extraction efficiencies of PAHs in the newly prepared PAHs-contaminated clay samples in this study.

Type of metal ions	PHE^a	ANT^a	B[a]A^a	PYR^a	B[a]P^a
Fe(III)	98.7%	97.8%	98.0%	99.7%	99.2%
Cu(II)	97.9%	98.5%	97.8%	98.0%	99.1%
Ni(II)	98.5%	98.2%	99.4%	97.7%	98.5%
Co(II)	99.1%	99.1%	98.7%	98.2%	97.9%
Zn(II)	98.3%	99.3%	98.1%	98.2%	98.7%

^aPhenanthrene (PHE), anthracene (ANT), benzo[a]anthracene (B[a]A), pyrene (PYR), and benzo[a]pyrene (B[a]P).

Table S2. Oxidation potential, ionization potential (IP), and half-wave potential ($E_{1/2}$) of polycyclic aromatic hydrocarbons (PAHs) and observed first-order rate constants (k_{obs} , d^{-1}) for decay of PAHs on various types of metal ion-containing modified clays.

PAH	Structure	Abbreviation	Oxidation Potential (w SCE) ^b	IP	$E_{1/2}$ (V)	k_{obs} (d^{-1})				
						Fe(III)	Cu(II)	Ni(II)	Co(II)	Zn(II)
Phenanthrene		PHE	1.67	7.89	1.50 ^a	~ 0	~ 0	~ 0	~ 0	~ 0
Anthracene		ANT	1.37	7.44	1.09 ^a	1.082±0.053	0.528±0.038	0.050±0.007	0.038±0.003	~ 0
Benzo[a]anthracene		B[a]A	1.44	7.45	1.18 ^a	0.503±0.014	0.171±0.007	0.039±0.007	0.030±0.003	~ 0
Pyrene		PYR	1.36	7.43	1.16 ^a	1.336±0.076	0.278±0.035	0.048±0.003	0.034±0.004	~ 0
Benzo[a]pyrene		B[a]P	1.16	7.12	0.94 ^a	2.424±0.235	1.452±0.114	0.052±0.004	0.037±0.001	0.023±0.001
^a Reference [1]										

^aPysh, E.S.; Yang, N.C. Polarographic Oxidation Potentials of Aromatic Compounds. *J. Am. Chem. Soc.*, **1963**, 85, 2124.

^bSCE-Standard calomel electrode

Table S3. Values of potential energy surface (PES) (kcal mol⁻¹) for the interactions of selected polycyclic aromatic hydrocarbons (PAHs) with different metal ions.

		PHE ^a	ANT ^a	B[a]A ^a	PYR ^a	B[a]P ^a
Fe(III)	S1→S2	41.16	19.76	22.91	15.34	14.52
	S2→S3	-22.88	-25.89	-25.72	-29.74	-31.57
	S3→S4	67.39	28.36	14.39	11.35	5.83
	S4→S5	-9.69	-21.99	-14.72	-15.83	-15.51
Cu(II)	S1→S2	43.93	20.08	26.83	23.87	19.83
	S2→S3	-15.27	-23.12	-22.97	-23.96	-25.81
	S3→S4	41.97	23.86	19.54	17.51	22.63
	S4→S5	-19.69	-38.00	-32.42	-31.62	-24.94
Ni(II)	S1→S2	43.18	25.14	27.96	26.43	21.64
	S2→S3	-13.88	-23.22	-20.51	-20.46	-23.49
	S3→S4	55.78	25.77	13.65	15.74	27.04
	S4→S5	-18.51	-33.76	-29.32	-33.44	-18.88
Co(II)	S1→S2	41.81	22.36	26.71	27.88	21.59
	S2→S3	-14.65	-21.87	-18.81	-17.36	-20.55
	S3→S4	46.74	23.48	20.36	20.32	34.14
	S4→S5	-13.46	-36.15	-34.48	-32.06	-19.71
Zn(II)	S1→S2	48.65	38.59	44.89	38.00	28.26
	S2→S3	1.07	-18.92	-16.27	-16.44	-19.70
	S3→S4	63.13	19.15	26.54	26.75	31.53
	S4→S5	-2.46	-22.82	-22.34	-15.58	-19.61

^aPhenanthrene (PHE), anthracene (ANT), benzo[a]anthracene (B[a]A), pyrene (PYR), and benzo[a]pyrene (B[a]P)

Table S4. First-order decay rate constants and 1/e life-times of EPFR signals during anthracene (ANT) and benzo[a]pyrene (B[a]P) transformation on metal ion-modified clays.

Type of radicals	ANT		B[a]P	
	$k_{\text{obs}}, \text{d}^{-1}$	Life-times ($t_{1/e}$)	$k_{\text{obs}}, \text{d}^{-1}$	Life-times ($t_{1/e}$)
Fe(III)	0.044±0.003	22.73±1.55	—	—
Cu(II)	0.047±0.005	21.28±2.26	0.073±0.005	13.70±0.94
Ni(II)	0.054±0.004	18.52±1.37	0.023±0.002	43.48±1.89
Co(II)	0.085±0.007	11.76±0.97	0.017±0.001	58.82±3.46

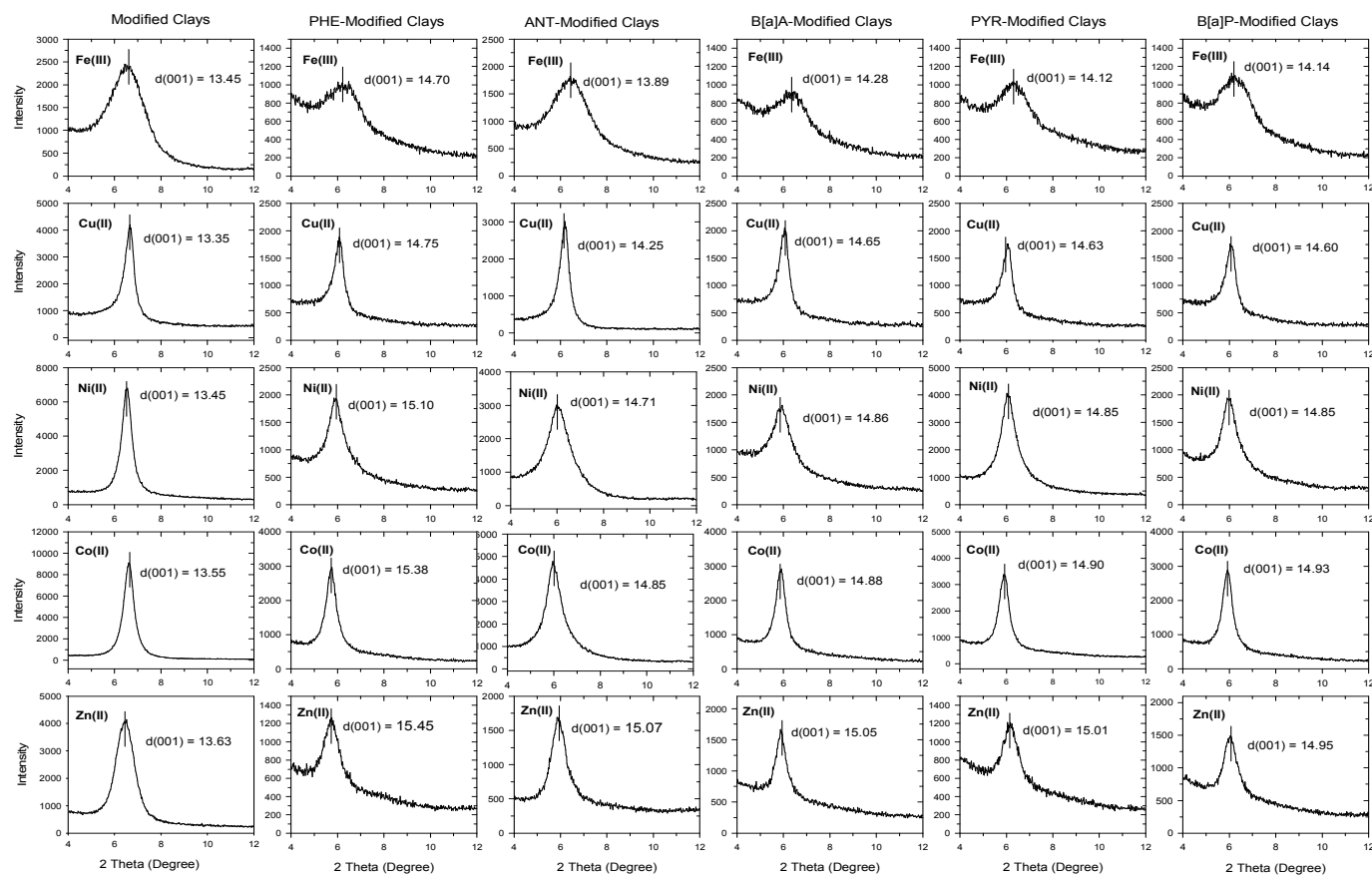


Figure S1. X-ray diffraction patterns of cations-modified smectite and their interactions with different PAHs.

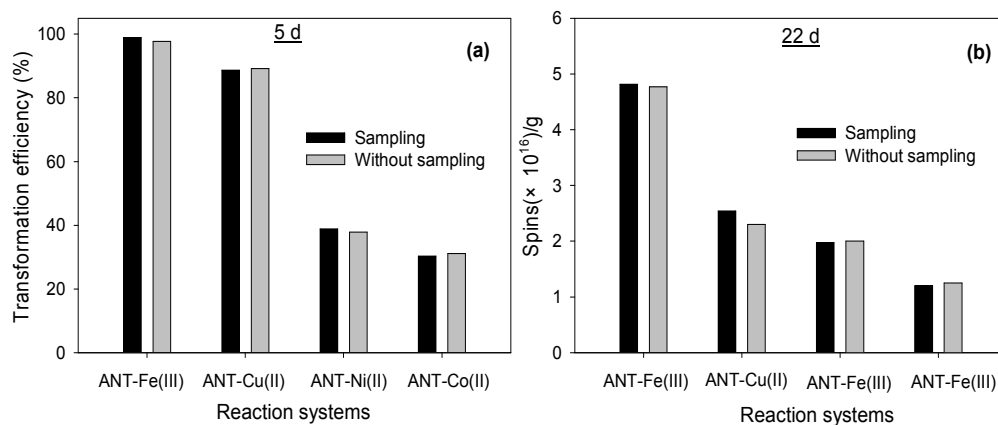


Figure S2. Samplings at two different preselected reaction times and without sampling. (a) transformation efficiency of ANT on metal ions-modified clays and (b) formation of EPFRs on metal ions-modified clays. “Without sampling” means not opening the desiccator until the end point, and “sampling” means sampling at preselected reaction time.

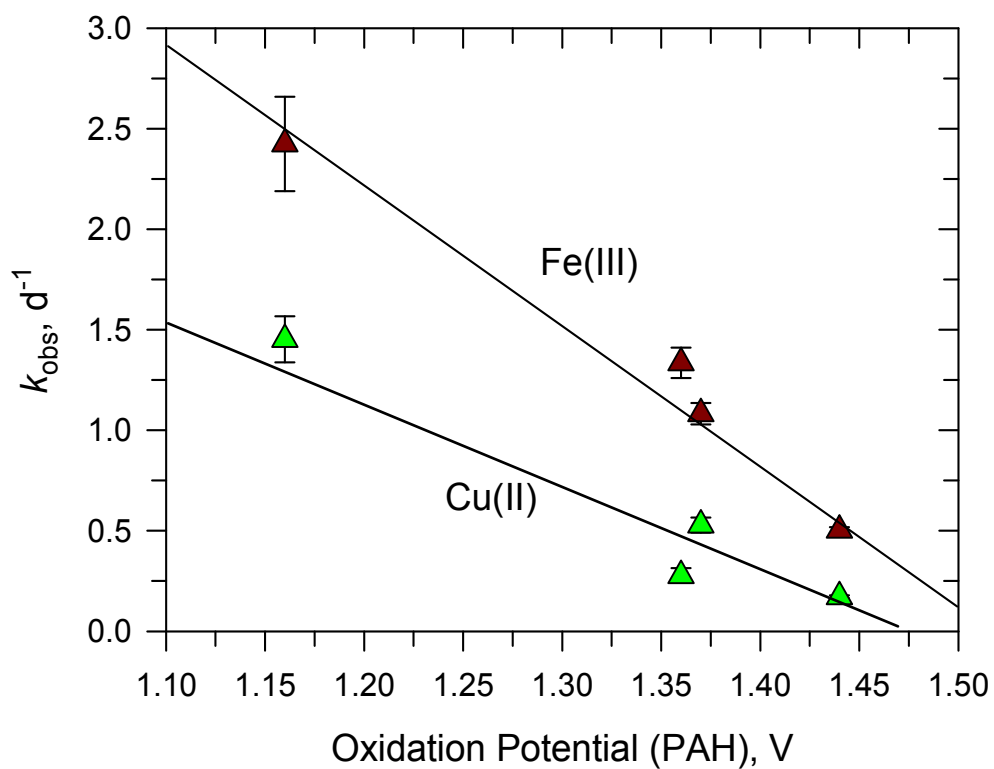


Figure S3. The relationship between observed first-order rate constant (k_{obs} , d^{-1}) for the degradation of anthracene (ANT), benzo[a]anthracene (B[a]A), pyrene (PYR), and benzo[a]pyrene (B[a]P) on Fe(III) and Cu(II)-modified clays and oxidation potential of PAHs.

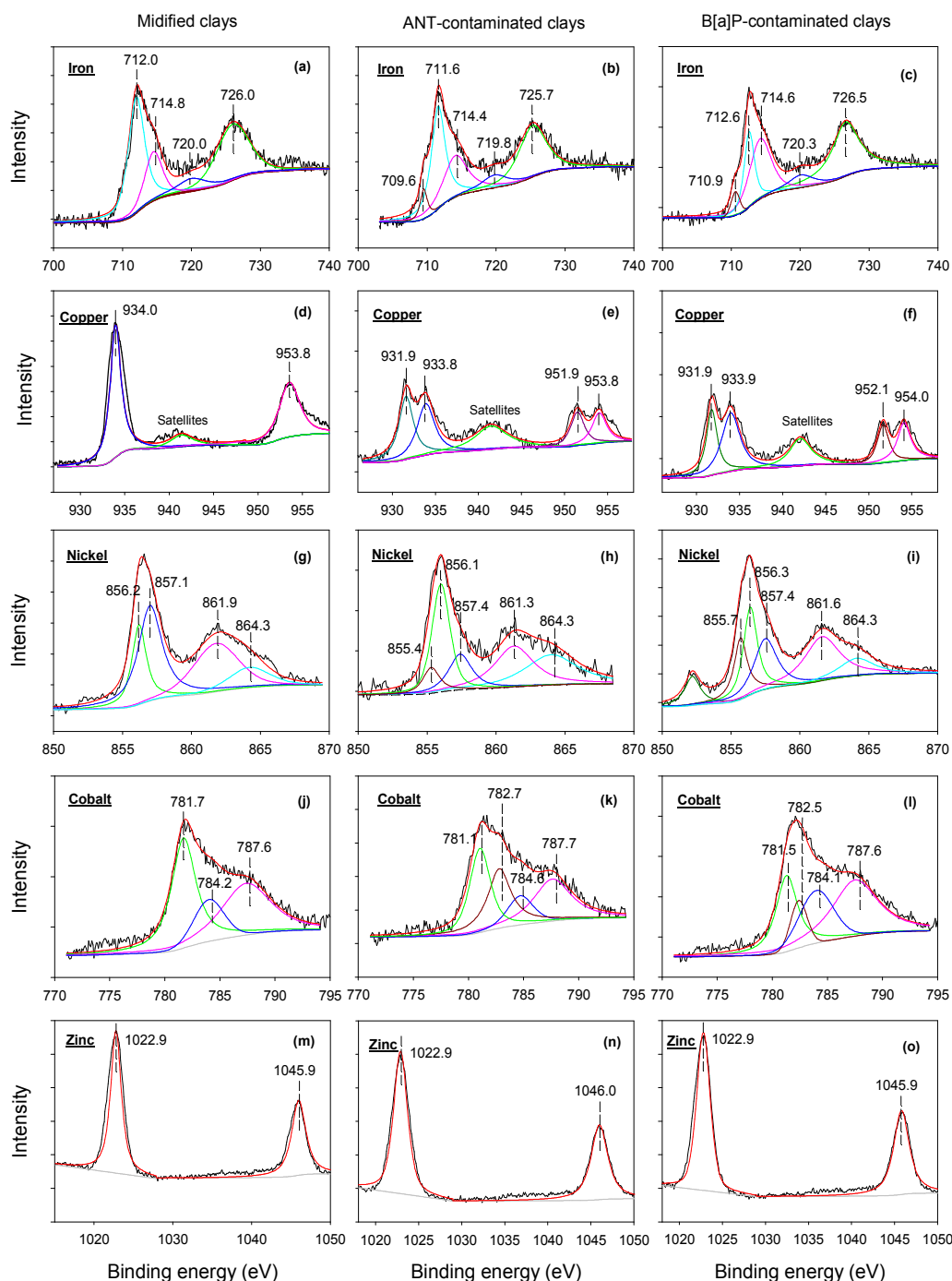


Figure S4. X-ray photoelectron spectra (XPS) of modified clays without PAHs (a, d, g, j, and m), ANT-contaminated clays (b, e, h, k, and n), and B[a]P-contaminated clays (c, f, i, l, and o) after 10 d. Fe(III)-montmorillonite – (a), (b), and (c); Cu(II)-montmorillonite – (d), (e), and (f); Ni(II)-montmorillonite – (g), (h), and (i); Co(II)-montmorillonite – (j), (k), and (l); and Zn(II)-montmorillonite – (m), (n), and (o). Abbreviations: ANT, anthracene; B[a]P, benzo[a]pyrene.

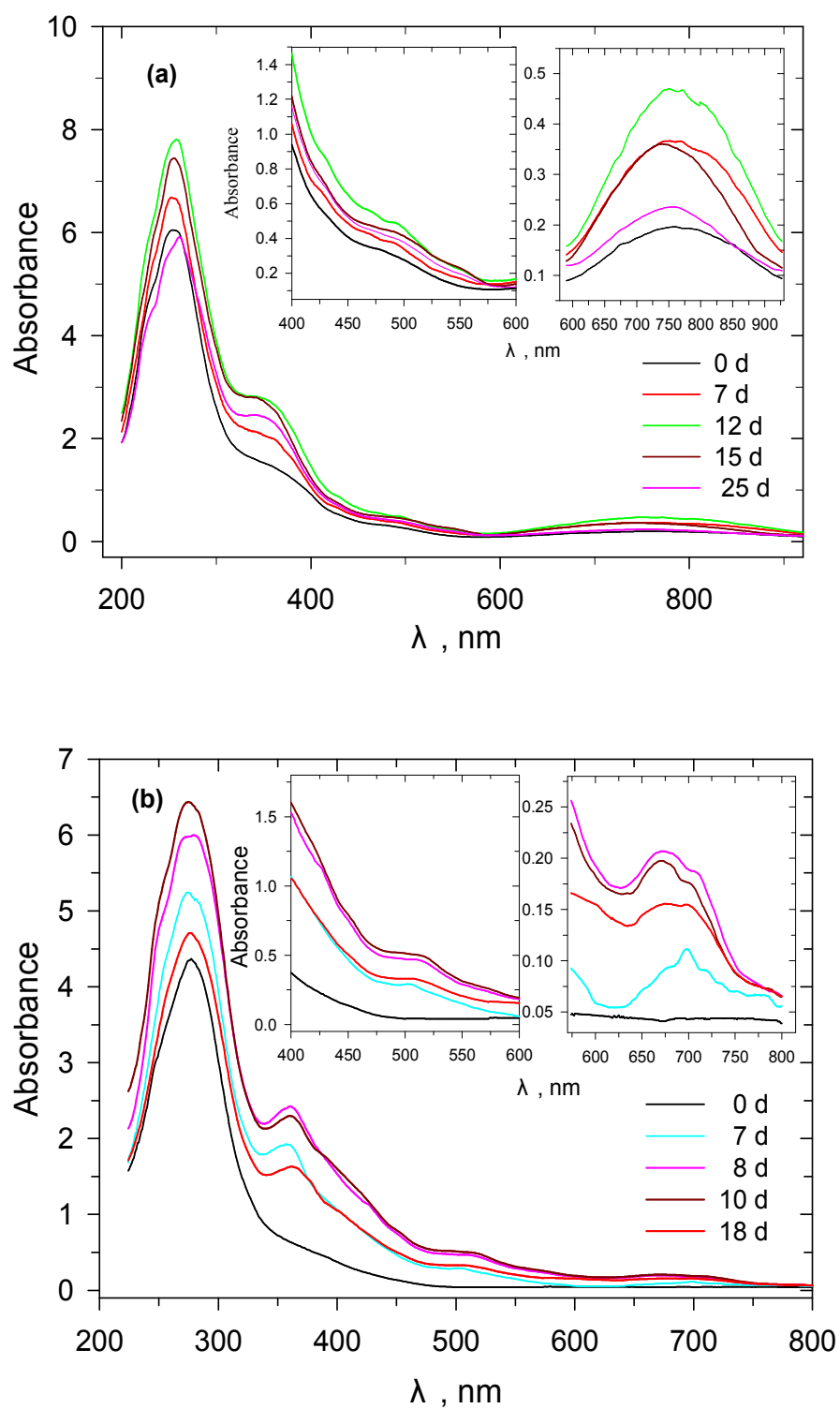
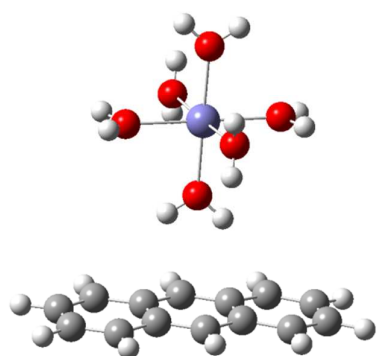
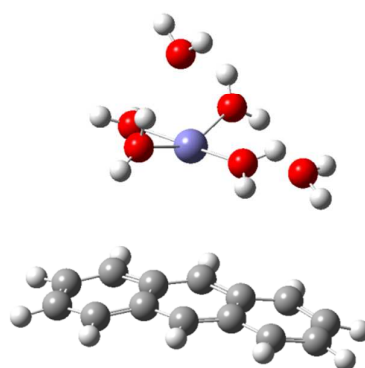


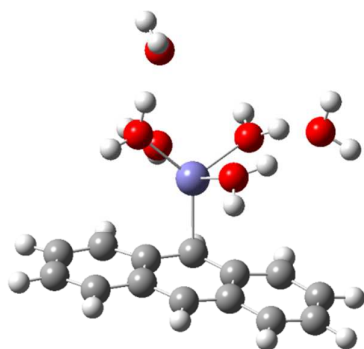
Figure S5. UV-Vis diffuse reflectance spectra of the reaction systems of (a) anthracene-contaminated Fe(III)-clay and (b) benzo[a]pyrene-contaminated Cu(II)-clay.



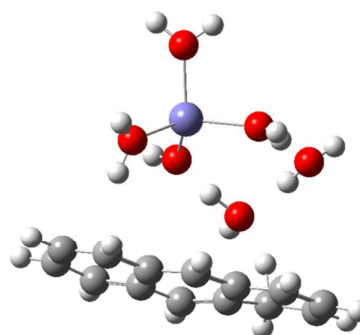
S 1



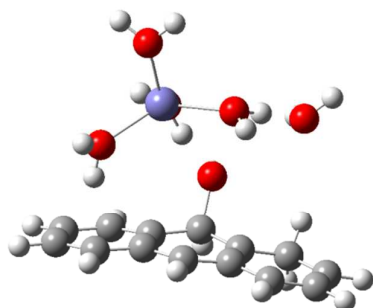
S 2



S 3



S 4



S 5

Figure S6. optimized structures during the interaction between ANT and Fe species.

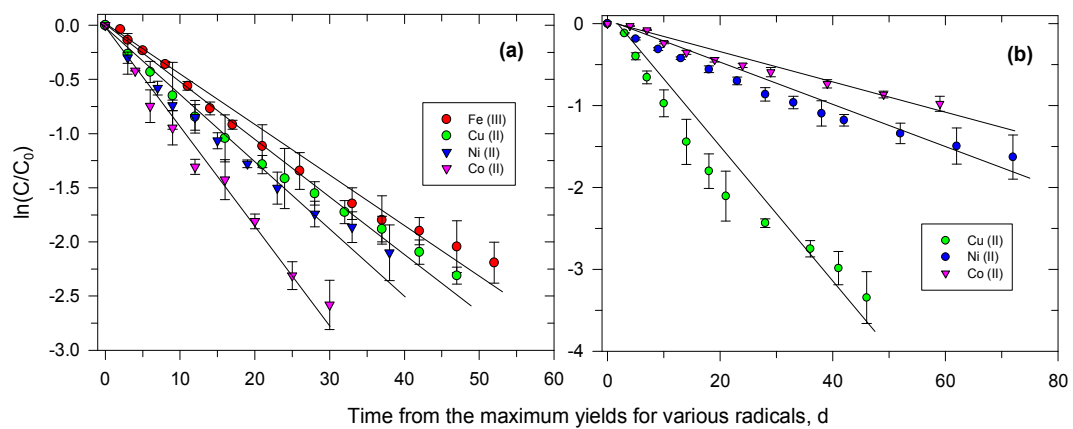


Figure S7. The decay electron paramagnetic resonance (EPR) signals of anthracene (ANT) and benzo[a]pyrene (B[a]P) are depicted from the reaction time at their highest yield.